Chapter 11

Partially Coherent Vortex Beam: From Theory to Experiment

Xianlong Liu, Lin Liu, Yahong Chen and Yangjian Cai

Additional information is available at the end of the chapter

http://dx.doi.org/10.5772/66323

Abstract

Partially coherent vortex beam exhibits some unique and interesting properties, for example, correlation singularities (i.e., ring dislocations) exist in its correlation function, and one can determine the magnitude of the topological charge of the vortex phase from the number of the ring dislocations. Modulating the coherence of a vortex beam provides a convenient way for shaping its focused beam spot, which is useful for material processing and optical trapping. Furthermore, a partially coherent vortex beam has an advantage over a partially coherent beam without vortex phase for reducing turbulence-induced scintillation, which will be useful in free-space optical communications. We introduce recent theoretical and experimental developments on partially coherent vortex beams.

Keywords: partially coherent vortex beam, generation, propagation, application

1. Introduction

Coherence is an important property of a light beam, which has been investigated widely in the past few decades [1]. Coherence can be regarded as a consequence of correlations between the components of the fluctuating electric field at two or more points. Light beam with low coherence is called partially coherent beam, and such beam has an advantage over a coherent beam in many applications, such as optical imaging [2–4], optical trapping [5, 6], free-space optical communications [7, 8], laser radar systems [9, 10] and remote sensing [11]. Before 2000, most literatures on partially coherent beam were focused on the conventional partially coherent beam named Gaussian Schell-model (GSM) beam [12–16], whose intensity and degree of coherence satisfy Gaussian distributions. Since 2000, partially coherent beams with prescribed

phase, state of polarization and degree of coherence were investigated widely due to their extraordinary properties and potential applications [17–31].

Phase is another important property of a light beam, which is characterized by the wavefront on propagation. Conventional Gaussian beam carries customary quadratic phase with spherical wavefront. Vortex beam, such as Laguerre-Gaussian beam, carries a vortex phase with helical wavefront. The intensity in the vortex beam center is zero while the phase is undefined, and this point is called phase singularity. In 1992, Allen et al. found that the vortex beam carries an orbital angular momentum (OAM) of $l\hbar$ with l being the topological charge [32]. Since then, numerous efforts have been devoted to vortex beams, and such beams have been applied in many applications [33–42], such as atom and particle trapping, optical tweezer, quantum information process, and laser cooling.

Vortex beam with low coherence is called partially coherent vortex beam, which was first proposed by Gori et al. [43]. Later, various partially coherent vortex beams were introduced [44–54]. Partially coherent vortex beam differs in many aspects from a coherent vortex beam, and it exhibits some unique interesting properties, for example, correlation singularities (i.e., ring dislocations) exist in its correlation function (i.e., cross-spectral density or degree of coherence) [47, 55–59]. Here the correlation singularity is defined as the point where the value of the cross-spectral density or degree of coherence equal zero, while the corresponding phase is undefined. Recently, more and more attention is being paid to partially coherent vortex beams [60–73], more interesting and useful results are being revealed. In this chapter, we will introduce recent theoretical and experimental developments on partially coherent vortex beams.

2. Theoretical models for various partially coherent vortex beams

There are different types of partially coherent vortex beams, such as partially coherent beam with helicoidal modes [43], partially coherent vortex beam with a separable phase [44, 45], Gaussian Schell-model vortex (GSMV) beam [46], partially coherent LG_{0l} beam [47, 48], partially coherent LG_{pl} beam [49], partially coherent Bessel-Gaussian beam [50], special correlated partially coherent vortex beam [51, 52] and vector partially coherent vortex beam [53, 54]. Here we only introduce some models which can be realized in experiment easily.

A scalar partially coherent beam can be characterized by the cross-spectral density (CSD) in the space-frequency domain or mutual intensity in the space-time domain [1]. For a GSMV beam, its CSD in the source plane is expressed as follows [46]:

$$W(r_1, r_2, \varphi_1, \varphi_2) = \exp\left[-\frac{r_1^2 + r_2^2}{4\sigma_0^2} - \frac{r_1^2 + r_2^2 - 2r_1 r_2 \cos(\varphi_1 - \varphi_2)}{2\delta_0^2} + il(\varphi_1 - \varphi_2)\right], \tag{1}$$

where r and φ are the radial and azimuthal (angle) coordinates, σ_0 and δ_0 denotes the beam width and coherence width of a GSMV beam, respectively, and l denotes the topological charge. When $\delta_0 = \infty$, the GSMV beam reduces to a coherent Gaussian vortex beam.

The CSD of a partially coherent LG_{pl} beam in the source plane is expressed as follows [49]:

$$W(r_1, r_2, \varphi_1, \varphi_2) = \left(\frac{\sqrt{2}r_1}{\omega_0}\right)^l \left(\frac{\sqrt{2}r_2}{\omega_0}\right)^l L_p^l\left(\frac{2r_1^2}{\omega_0^2}\right) L_p^l\left(\frac{2r_2^2}{\omega_0^2}\right) \exp\left(-\frac{r_1^2 + r_2^2}{\omega_0^2}\right) \exp\left(il\varphi_1 - il\varphi_2\right) \times \exp\left[-\frac{r_1^2 + r_2^2 - 2r_1 r_2 \cos\left(\varphi_1 - \varphi_2\right)}{2\delta_0^2}\right], \tag{2}$$

where L_p^l denotes the Laguerre polynomial with mode orders p and l. When $p = 0$, Eq. (2) reduces to the CSD of a partially coherent LG_{0l} beam [47, 48]. When $p = 0$ and $l = 0$, Eq. (2) reduces to the CSD of the well-known GSM beam [12–16].

As a typical kind of special correlated partially coherent vortex beam, the CSD of a Laguerre-Gaussian correlated Schell-model vortex (LGCSMV) beam in the source plane is expressed as [51]:

$$W(\mathbf{r}_1, \mathbf{r}_2) = \exp\left[-\frac{\mathbf{r}_1^2 + \mathbf{r}_2^2}{4\sigma_0^2} - \frac{(\mathbf{r}_1 - \mathbf{r}_2)^2}{2\delta_0^2}\right] L_n^0\left[\frac{(\mathbf{r}_1 - \mathbf{r}_2)^2}{2\delta_0^2}\right] \exp\left[il(\varphi_1 - \varphi_2)\right]. \tag{3}$$

When $n = 0$, Eq. (3) reduces to the CSD of a GSMV beam.

A vector partially coherent beam can be characterized by the CSD matrix in space-frequency domain or the beam coherence-polarization matrix in the space-time domain [17]. The elements of the CSD matrix of a vector partially coherent vortex beam with uniform state of polarization named electromagnetic Gaussian Schell-model vortex (EGSMV) beam in the source plane are given as [53]:

$$W_{\alpha\beta}(\mathbf{r}_1, \mathbf{r}_2) = A_\alpha A_\beta B_{\alpha\beta} \exp\left[-\frac{\mathbf{r}_1^2}{4\sigma_\alpha^2} - \frac{\mathbf{r}_2^2}{4\sigma_\beta^2} - \frac{(\mathbf{r}_1 - \mathbf{r}_2)^2}{2\delta_{\alpha\beta}^2}\right] \exp\left[il(\varphi_1 - \varphi_2)\right], \tag{4}$$

where A_x and A_y are the amplitudes of x and y components of the electric field, respectively. σ_i is the r.m.s width of the intensity distribution along the i direction, δ_{xx}, δ_{yy} and δ_{xy} are the r.m.s widths of autocorrelation function of the x components of the electric field, of the y components of the electric field and of the mutual correlation function of x and y components of the electric field, respectively. $B_{xx} = B_{yy} = 1$, $B_{xy} = |B_{xy}| \exp\left(i\phi_{xy}\right)$ is the complex correlation coefficient between the x and y components of the electric field with ϕ_{xy} being the phase difference between the x and y components. The nine real parameters A_x, A_y, σ_x, σ_y, δ_{xx}, δ_{yy}, δ_{xy}, $|B_{xy}|$, ϕ_{xy} of an EGSMV beam are shown to satisfy several intrinsic constraints and obey some simplifying assumptions [17].

The elements of the CSD matrix of a vector partially coherent vortex beam with non-uniform state of polarization named radially polarized partially coherent vortex beam in the source plane are expressed as [54]:

$$W_{xx}(r_1,\varphi_1,r_2,\varphi_2)=\frac{r_1r_2\cos\varphi_1\cos\varphi_2}{4\sigma_0^2}T(r_1,\varphi_1,r_2,\varphi_2), \tag{5}$$

$$W_{xy}(r_1,\varphi_1,r_2,\varphi_2)=\frac{r_1r_2\cos\varphi_1\sin\varphi_2}{4\sigma_0^2}T(r_1,\varphi_1,r_2,\varphi_2), \tag{6}$$

$$W_{yx}(r_1,\varphi_1,r_2,\varphi_2)=W_{xy}^*(r_2,\varphi_2,r_1,\varphi_1), \tag{7}$$

$$W_{yy}(r_1,\varphi_1,r_2,\varphi_2)=\frac{r_1r_2\sin\varphi_1\sin\varphi_2}{4\sigma_0^2}T(r_1,\varphi_1,r_2,\varphi_2), \tag{8}$$

with

$$T(r_1,\varphi_1,r_2,\varphi_2)=\exp\left[-\frac{r_1^2+r_2^2-2r_1r_2\cos(\varphi_1-\varphi_2)}{2\delta_0^2}-\frac{r_1^2+r_2^2}{4\sigma_0^2}-il\varphi_1+il\varphi_2\right]. \tag{9}$$

3. Propagation of partially coherent vortex beams

Propagation of a partially coherent vortex beam in free space can be studied with the help of the well-known Huygens-Fresnel integral, and propagation of a partially coherent vortex beam through a paraxial ABCD optical can be studied with the help of the following generalized Collins formula [74]:

$$\begin{aligned}W(\rho_1,\phi_1,\rho_2,\phi_2)=&\frac{1}{\lambda^2BB^*}\exp\left(\frac{ikD^*\rho_2^2}{2B^*}-\frac{ikD\rho_1^2}{2B}\right)\int_0^{2\pi}\int_0^{2\pi}\int_0^{\infty}\int_0^{\infty}W(r_1,\varphi_1,r_2,\varphi_2)\\&\times\exp\left\{ik\left[\frac{A^*r_2^2}{2B^*}-\frac{Ar_1^2}{2B}+\frac{\rho_1r_1}{B}\cos(\phi_1-\varphi_1)\right]\right.\\&\left.\times\exp\left[-ik\frac{\rho_2r_2}{B^*}\cos(\phi_2-\varphi_2)\right]r_1r_2dr_1dr_2d\varphi_1d\varphi_2\right.,\end{aligned} \tag{10}$$

where $W(\rho_1,\phi_1,\rho_2,\phi_2)$ is the cross-spectral density in the receiver plane, $k=2\pi/\lambda$ is the wave number with λ being the optical wavelength, A, B, C, and D are the elements of the transfer matrix of the paraxial optical system, the asterisk denotes the complex conjugate.

Propagation of a partially coherent vortex beam through turbulent atmosphere can be studied with the help of the following generalized Huygens-Fresnel integral [75]

$$\begin{aligned}W(\boldsymbol{\rho}_1,\boldsymbol{\rho}_2)=&\int_{-\infty}^{\infty}\int_{-\infty}^{\infty}\int_{-\infty}^{\infty}\int_{-\infty}^{\infty}W(\boldsymbol{r}_1,\boldsymbol{r}_2)\exp\left[-\frac{ik(\boldsymbol{\rho}_1-\boldsymbol{r}_1)^2}{2z}+\frac{ik(\boldsymbol{\rho}_2-\boldsymbol{r}_2)^2}{2z}\right]\\&\exp\left\{-\frac{\pi^2k^2z}{3}\left[(\boldsymbol{\rho}_1-\boldsymbol{\rho}_2)^2+(\boldsymbol{\rho}_1-\boldsymbol{\rho}_2)\cdot(\boldsymbol{r}_1-\boldsymbol{r}_2)+(\boldsymbol{r}_1-\boldsymbol{r}_2)^2\right]\int_0^{\infty}\kappa^3\Phi_n(\kappa)d\kappa\right\}d^2\boldsymbol{r}_1d^2\boldsymbol{r}_2.\end{aligned} \tag{11}$$

Here $\Phi_n(\kappa)$ is the one-dimensional power spectrum of the refractive-index fluctuations of the atmospheric turbulence, $\boldsymbol{\kappa}$ is the spatial frequency.

http://dx.doi.org/10.5772/66323

The average intensity and the degree of coherence of a partially coherent vortex beam in the receiver plane are obtained as:

$$I(\boldsymbol{\rho}) = W(\boldsymbol{\rho},\boldsymbol{\rho}), \quad \mu(\boldsymbol{\rho}_1,\boldsymbol{\rho}_2) = \frac{W(\boldsymbol{\rho}_1,\boldsymbol{\rho}_2)}{\sqrt{I(\boldsymbol{\rho}_1)I(\boldsymbol{\rho}_2)}}. \tag{12}$$

Coherent vortex beam displays dark hollow beam profile in the source plane or on propagation in free space. For a partially coherent vortex beam, it also displays dark hollow beam profile in the source plane, while its beam profile varies on propagation due to the degradation caused by the source spatial coherence, and one can shape the beam spot of a partially coherent vortex beam in the focal plane through varying the initial coherence width, for example, the beam profile of the focused beam spot gradually transforms from a dark hollow beam profile to a flat-topped beam profile and finally to a Gaussian beam profile when the coherence width gradually decreases (see **Figure 1**). Furthermore, when the initial coherence width is fixed, one also can shape the beam spot of a partially coherent vortex beam through varying its initial topological charge because the topological charge plays a role of anti-degradation caused by the coherence [46].

For a vector partially coherent beam with nonuniform state of polarization (i.e., radially polarized partially coherent beam), it is known that such beam always displays radial polarization on propagation (see **Figure 2(a1)–(e1)**) although its degree of polarization varies. For a radially polarized partially coherent vortex beam, one finds from [54] that the vortex phase induces changes of not only the degree of polarization but also the state of polarization (see **Figure 2(a2)–(e2)** and **(a3)–(e3)**) besides rotation of the beam spot, that is, radial polarization disappears and elliptical polarization appears on propagation. The state of polarization displays left-handed elliptical polarization around the beam center and right-handed elliptical polarization outside of the beam center for l >0, and the handedness of the polarization ellipse

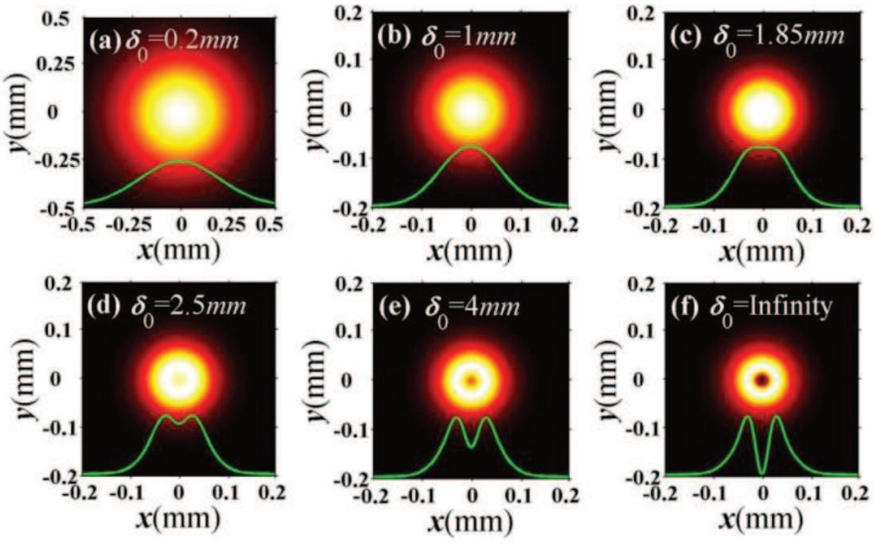

Figure 1. Average intensity of a partially coherent LG_{0l} beam with l =2 in the focal plane for different values of the initial coherence width δ_0.

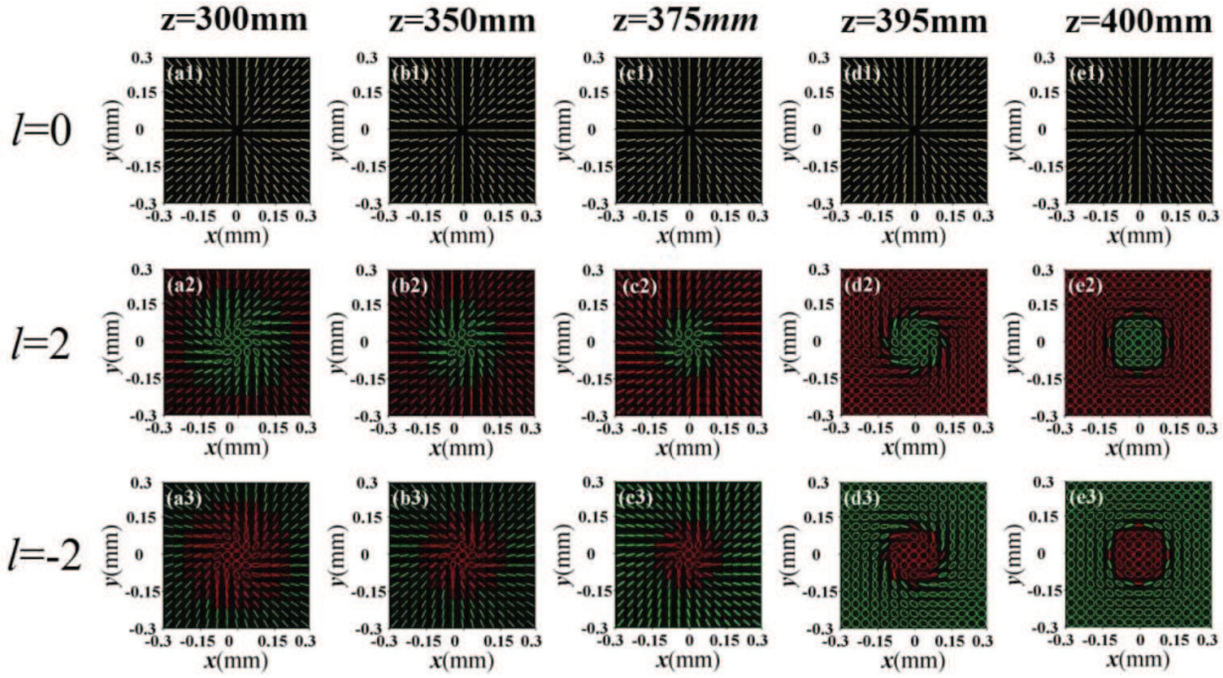

Figure 2. Changes of the state of polarization of a focused radially polarized partially coherent vortex beam on propagation for different values of the topological charge *l*.

is reversed for $l < 0$. Furthermore, the polarization ellipse rotates clockwise for $l > 0$ and anticlockwise for $l < 0$ on propagation. Thus, modulating the magnitude and sign of the topological charge of the vortex phase provides a convenient way for modulating the polarization properties of a vector partially coherent vortex beam. What is more, the phenomenon of vortex phase-induced changes of the state of polarization of a radially polarized partially coherent beam may be used to detect a phase object.

Coherent vortex beam carries phase singularity in the source plane and on propagation. Phase singularity is defined as the point where the intensity is zero while the phase is undefined. When the spatial coherence of a vortex beam is reduced, the dark hollow beam profile disappears on propagation due to the degradation caused by the coherence (see **Figure 3(a)–(c)**). Thus, a partially coherent vortex beam does not carry phase singularity on propagation, while an interesting correlation singularity named ring dislocation appears (see **Figure 3(d)–(f)**). Here the correlation singularity is defined as the point where the amplitude of the cross-spectral density $\boldsymbol{W}(\boldsymbol{\rho}, -\boldsymbol{\rho})$ or degree of coherence $\boldsymbol{\mu}(\boldsymbol{\rho}, -\boldsymbol{\rho})$ is zero while the corresponding phase is undefined. It was demonstrated in [47] both theoretically and experimentally that correlation singularity (i.e., ring dislocation) exists in a partially coherent vortex beam on propagation. One finds from **Figure 3(d)–(f)** that the ring dislocation becomes more obvious with the decrease of the spatial coherence.

The study of optical beam propagation in turbulent atmosphere is a venerable subject. It is known that the turbulence induces scintillation (i.e., intensity fluctuations), beam wander and deformation of laser beam, which impedes the applications of free-space optical communications, optical imaging and remote sensing. Propagation properties of a partially coherent beam

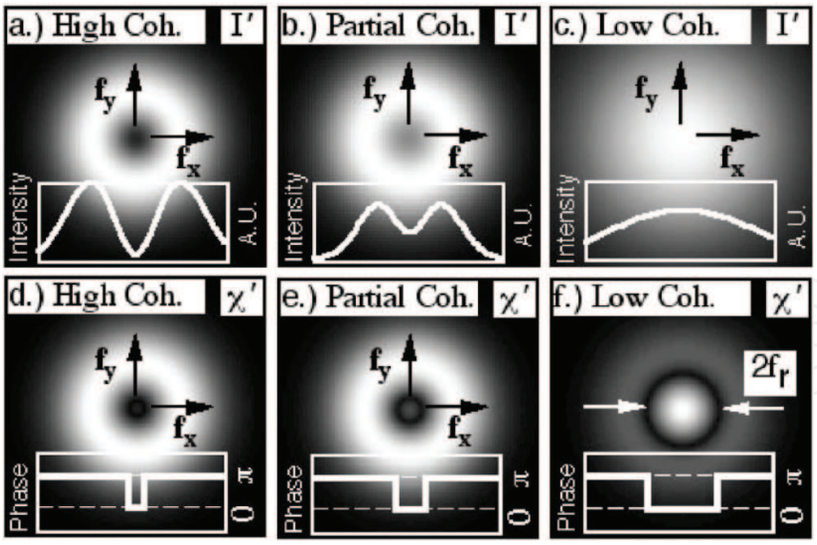

Figure 3. Far-field intensity distribution and corresponding amplitude and phase distribution of the correlation function of a partially coherent LG_{0l} beam.

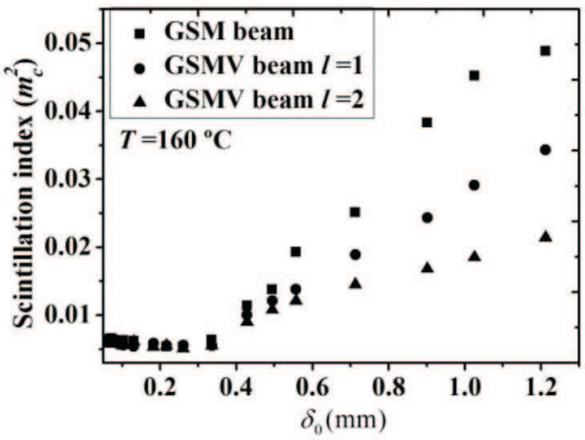

Figure 4. Experimental results of the scintillation index of a GSM or GSMV beam (l = 1, 2) at the centroid versus the initial coherence width after propagating through thermal turbulence.

in turbulent atmosphere have been investigated in detail in the past few decades, and it was found that a GSM beam has an advantage over a coherent Gaussian beam for reducing turbulence-induced scintillation and degradation [7, 8]. The scintillation index of a beam in turbulent atmosphere is defined as follows:

$$m_c^2 = \langle I^2(\rho_x, \rho_y)\rangle / \langle I(\rho_x, \rho_y)\rangle^2 - 1, \tag{13}$$

where $I(\rho_x, \rho_y)$,$\langle I(\rho_x, \rho_y)\rangle$ and $\langle I^2(\rho_x, \rho_y)\rangle$ represent the instantaneous intensity, the average intensity and the intensity correlation function of the beam in the receiver plane.

Is it possible to further reduce turbulence-induced scintillation compared to GSM beam? Recently, propagation properties of a partially coherent vortex beam in turbulent atmosphere

have been investigated both theoretically and experimentally [60–62]. It was shown in [62] that a GSMV beam has an advantage over a GSM beam for further reducing turbulence-induced scintillation (see **Figure 4**). From **Figure 4**, one sees that the scintillation index of a GSMV beam or a GSM beam decreases with the decrease of initial coherence width δ_0, and the scintillation index of a GSMV beam is always smaller than that of a GSM beam unless the coherence width is very small ($\delta_0 < 0.35$mm). When the coherence width is very small, the scintillation index of a GSMV beam is almost the same with that of a GSM beam, and the phenomenon can be explained by the fact that the influence of the coherence on the scintillation index plays a dominant role, while the influence of the vortex phase is negligible when the coherence width is very small. Thus, the scintillation index of the GSMV beam with extremely low coherence is similar to that of a GSM beam.

4. Generation of partially coherent vortex beams

Up to now, many different methods have been developed to generate a coherent vortex beam, such as spiral phase plate [76], transverse mode selection [77], holographic grating [78], spatial light modulator [79], helical optical fiber [80] and uniaxial crystal [81], while only few papers were devoted to generation of partially coherent vortex beams [46–48, 51, 53, 54, 73].

One can generate a GSMV beam in experiment with the help of a rotating ground-glass disk, Gaussian amplitude filter and a spiral phase plate [46]. As shown in **Figure 5**, a focused laser beam generated by a He-Ne laser is reflected by a mirror and then illuminates a RGGD, producing a partially coherent beam with Gaussian statistics. The thin lens L_2 is used to collimate the transmitted light, and the GAF is used to transform the intensity of the transmitted light into a Gaussian profile. The transmitted light behind the GAF is a GSM beam. The coherence width of the GSM beam is determined by the focused beam spot size on the RGGD, which is controlled by the varying the distance between lens L_1 and RGGD. After passing

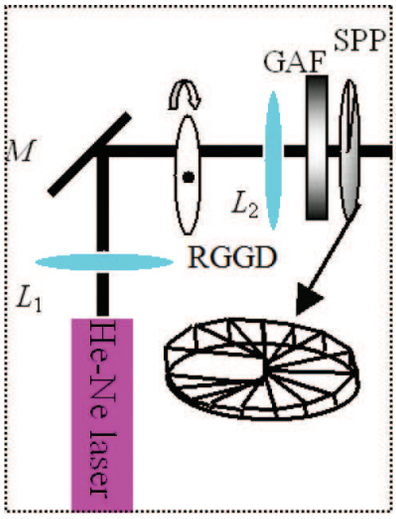

Figure 5. Experimental setup for generating a GSMV beam. L_1, L_2, thin lenses; M, mirror; RGGD, rotating ground-glass disk; GAF, Gaussian amplitude filter; SPP, spiral phase plate.

through a SPP located just behind the GAF, the GSM beam becomes a GSMV beam. It is true that the beam spot of the generated GSMV beam in the focal plane is shaped by varying its coherence width (see **Figure 6**).

One can generate a partially coherent LG_{pl} beam in experiment with the help of a rotating ground-glass disk, Gaussian amplitude filter and a SLM [48]. As shown in **Figure 7**, the RGGD and GAF are used to generate a GSM beam. The generated GSM beam goes toward a spatial light modulator (SLM), which acts as a grating with fork pattern designed by the method of computer-generated holograms. The first-order diffraction pattern of the beam reflected from the SLM is regarded as a partially coherent LG_{pl} beam and is selected out by a circular aperture.

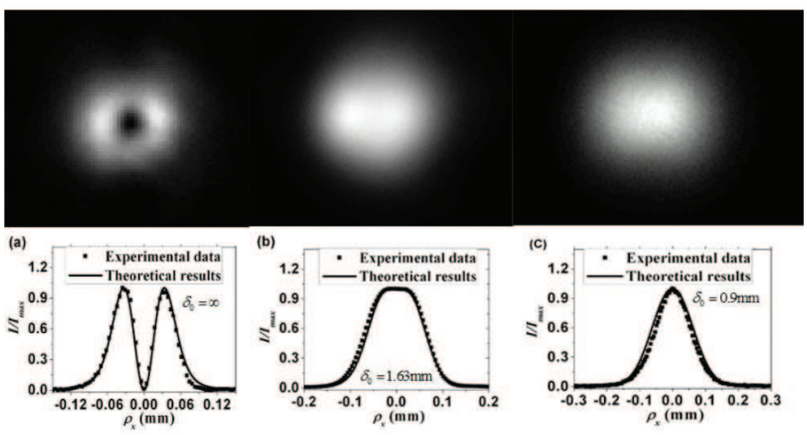

Figure 6. Experimental results of the focused intensity distribution and the corresponding cross line (dotted curve) of the generated GSMV beam for three different coherence widths. The solid curves are calculated by theoretical formulae.

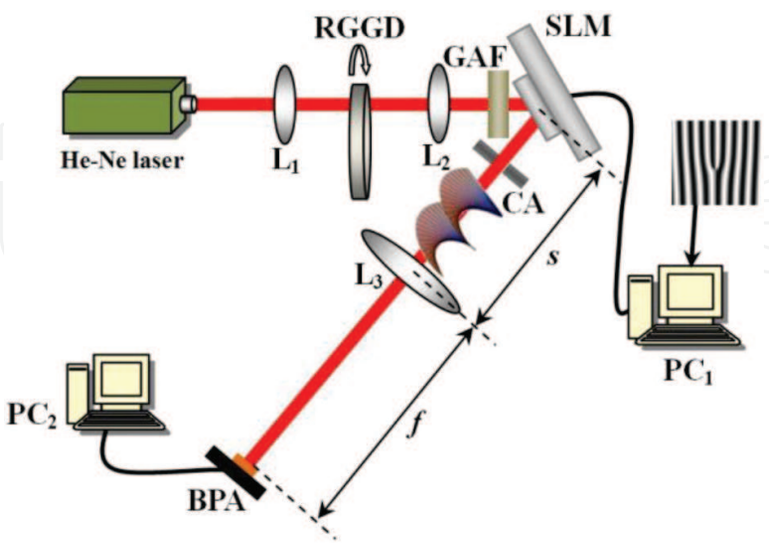

Figure 7. Experimental setup for generating a partially coherent LG_{pl} beam. L_1, L_2, L_3, thin lenses; RGGD, rotating ground-glass disk; GAF, Gaussian amplitude filter; SLM, spatial light modulator; CA, circular aperture; BPA, beam profile analyzer.

Figure 8 shows the experimental setup for generating a LGCSMV beam [25]. A beam emitted from the He-Ne laser passes through a beam expander, and then it goes toward a SLM. The first order of the beam from the SLM is a dark hollow beam and is selected out by a circular aperture. The generated dark hollow beam illuminates a RGGD, producing an incoherent

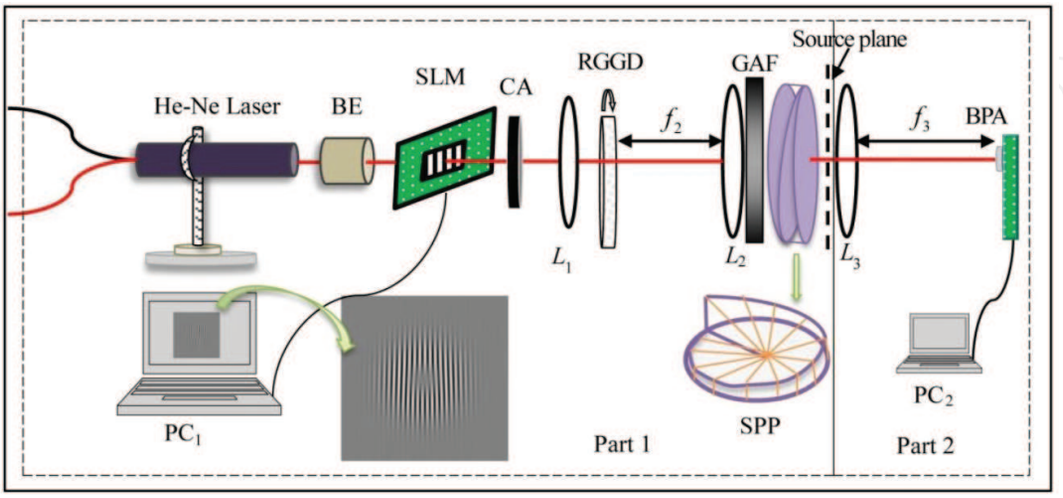

Figure 8. Experimental setup for generating a LGCSMV beam. BE, beam expander; SLM, spatial light modulator; CA, circular aperture; L_1, L_2, L_3, thin lenses; RGGD, rotating ground-glass disk; GAF, Gaussian amplitude filter; SPP, spiral phase plate; BPA, beam profile analyzer.

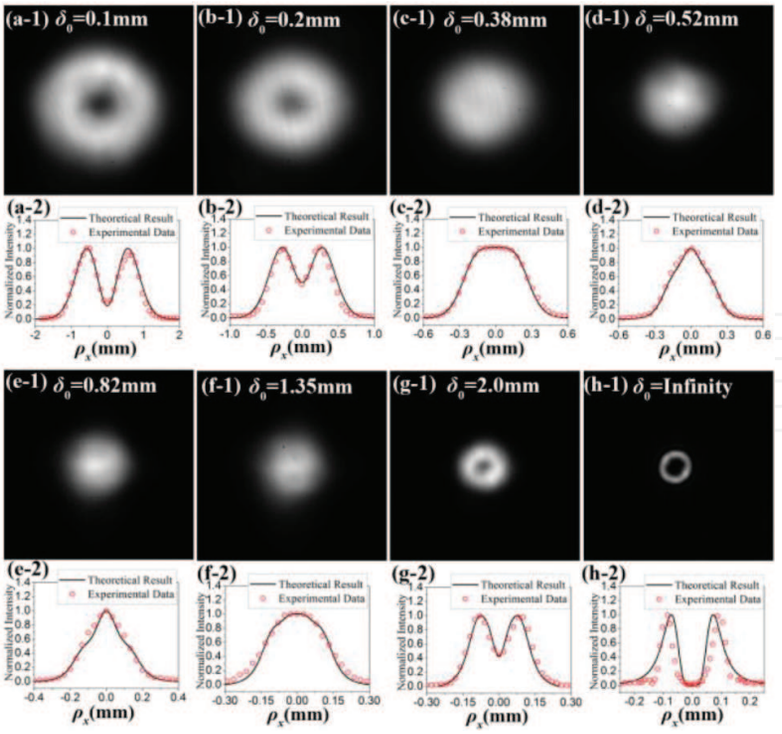

Figure 9. Experimental results of the intensity distribution and the corresponding cross line of the generated LGCSM vortex beam in the focal plane for different values of the coherence width. The solid curve denotes the theoretical results.

beam with dark hollow beam profile. After passing through free space with length f_2, the thin lens L_2, and the GAF, the generated incoherent dark hollow beam becomes a LGCSM beam. After passing through a SPP, the generated LGCSM beam becomes a LGCSMV beam. Due to the influence of the special correlation function, the LGCSMV beam exhibits interesting focusing properties, for example, the focused beam spot displays dark hollow beam profile when the coherence width is very large or very small, and displays flat-topped beam profile of Gaussian beam profile when the coherence width takes a middle value (see **Figure 9**), which are much different from the focusing properties of the conventional partially coherent vortex beam (see **Figures 1** and **6**).

In a similar way, experimental generation of an EGSMV beam and a radially polarized partially coherent vortex beam were reported in [53,54], respectively. It was shown that the vortex phase induces not only the rotation of the beam spot, but also the changes of the beam shape, the degree of polarization and the state of polarization. Furthermore, it was revealed that the vortex phase plays a role of resisting the coherence-induced degradation of the intensity distribution and the coherence-induced depolarization.

More recently, a new experimental technique is developed in [81] to generate partially coherent vortex beams with arbitrary azimuthal index using only a spatial light modulator (see **Figure 10**). This technique is based on digitally simulating the intrinsic randomness of broadband light passing through a spiral phase plate, and it provides control over the transverse coherence length, which will be useful for study of vector singularities in partially coherent fields or in the fields of optical communications and imaging systems where coherence plays a key role.

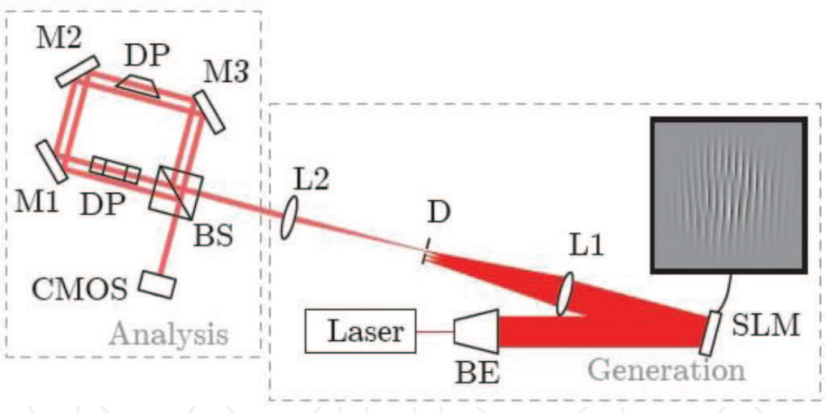

Figure 10. Experimental setup for digital generation of partially coherent vortex beam. HeNe Laser; BE: beam expander; L1–L2: lenses; D: iris diaphragm; SLM: spatial light modulator; BS: beam splitter; DP: Dove prism; M1–M3: mirrors; CMOS: camera.

5. Determination of the topological charge of a partially coherent vortex beam

It is known that a vortex beam carries an OAM of $l\hbar$ with l being the topological charge [32]. Different methods have been developed to determine or measure the topological charge (i.e.,

OAM) of a coherent vortex beam [82–88]. However, these methods are mainly based on measuring the intensity distribution of a vortex beam passing through different diffractive elements or intensity distribution produced by the interference of a vortex beam with a reference plane wave. For a partially coherent vortex beam, the conventional methods for measuring the topological charge will be invalid because the intensity distribution is seriously deformed, while fortunately, some methods have been proposed to measure or determine the topological charge of a partially coherent vortex beam based on the measurement of the correlation function recently [65–71].

For a coherent vortex beam, it is known from [88] that the number of dark rings in the Fourier transform of the intensity of a coherent vortex beam equals to the magnitude of the topological charge, thus one can determine the magnitude of the topological charge once we obtain the information of the intensity of a vortex beam. With the decrease of initial coherence width, the hollow profile of the intensity distribution of a vortex beam in the focal plane or in the far field disappears gradually and finally becomes a Gaussian beam profile (see **Figure 11(a-1)–(a-4)**), and the dark rings of the Fourier transform of the intensity distribution disappear (see **Figure 11(b-1)–(b-4)**). Then how to determine the topological charge of a partially coherent vortex beam? It is shown in [47] that the correlation function of a partially coherent vortex beam (i.e., partially coherent LG_{0l} beam) displays correlation singularity (i.e., ring dislocation) in the far field. Here the correlation function denotes the cross-spectral density $\boldsymbol{W}(\boldsymbol{\rho}, -\boldsymbol{\rho})$ or the degree of coherence $\boldsymbol{\mu}(\boldsymbol{\rho}, -\boldsymbol{\rho})$. Later in [65,66], it was revealed that for the number of ring dislocations of a partially coherent LG_{0l} beam in the focal plane or in the far field equals to the magnitude of the topological charge (see **Figure 12**). From **Figure 12**, one sees that the ring

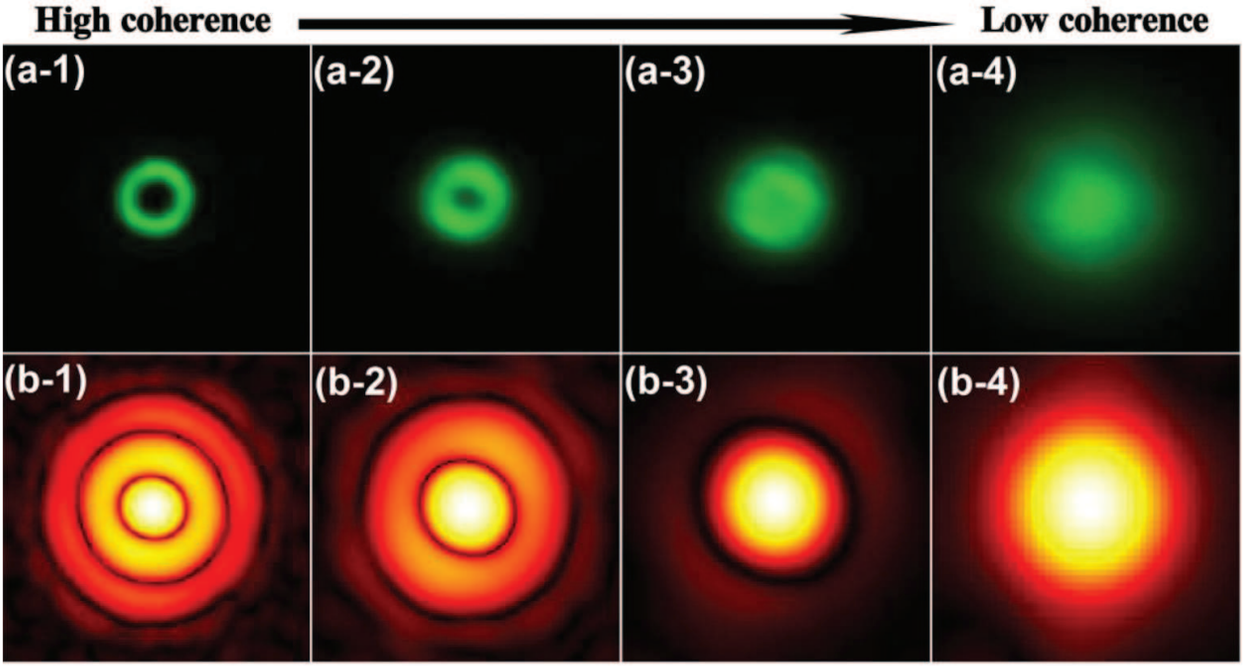

Figure 11. (a-1)–(a-4) Intensity distribution and (b-1)–(b-4) the corresponding Fourier transform of a partially coherent LG_{0l} beam with l =3 in the focal plane for different state of coherence.

http://dx.doi.org/10.5772/66323

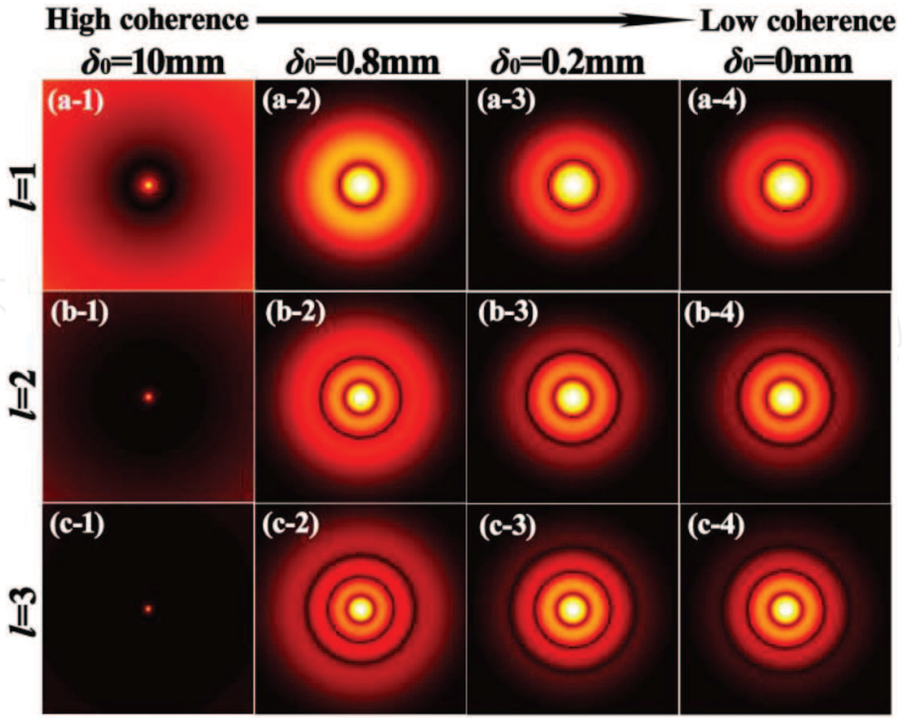

Figure 12. Distribution of the modulus of the degree of coherence of a partially coherent LG_{0l} beam with different values of the topological charge l in the focal plane for different state of coherence.

dislocations in the correlation function does not exist when initial coherence width is large, and the rings dislocations gradually appear with the decrease of the coherence, and such rings dislocations even exist in an incoherent LG_{0l} beam. Thus, one can determine the magnitude of the topological charge of a partially coherent or incoherent LG_{0l} beam through measuring its correlation function, and this phenomenon is confirmed experimentally in [67]. For a partially coherent LG_{pl} beam, it was demonstrated both theoretically [68] and experimentally [69] that the number of the ring dislocations equal to $2p+|l|$ (see **Figure 13**). Recently, it was predicted in [70] that one may determine p and l through measuring the double-correlation function, which is defined as $W(\rho, 2\rho)$ or $\mu(\rho, 2\rho)$.

Abovementioned literatures are confined to measure the magnitude of the topological charge of a partially coherent vortex beam. In fact, the sign of the topological charge of vortex phase also plays an important role in practical applications, for example, the sign of the vortex phase provides an additional degree of freedom for optical storage and communication [89, 90]. Recently, a simple method for simultaneous determination of the sign and the magnitude of the topological charge of a partially coherent LG_{0l} beam was proposed. This method is based on the measurement of the modulus of the degree of coherence of a partially coherent LG_{0l} beam after propagating through a couple of cylindrical lenses (see **Figure 14**). It was found that the distribution of the modulus of the degree of coherence becomes anisotropic, and it rotates anti-clockwise (or clockwise) during propagation when the sign of the topological charge is positive (or negative), furthermore, the modulus of the degree of coherence displays fringes distribution within certain propagation distances and the number of the bring fringes equals to

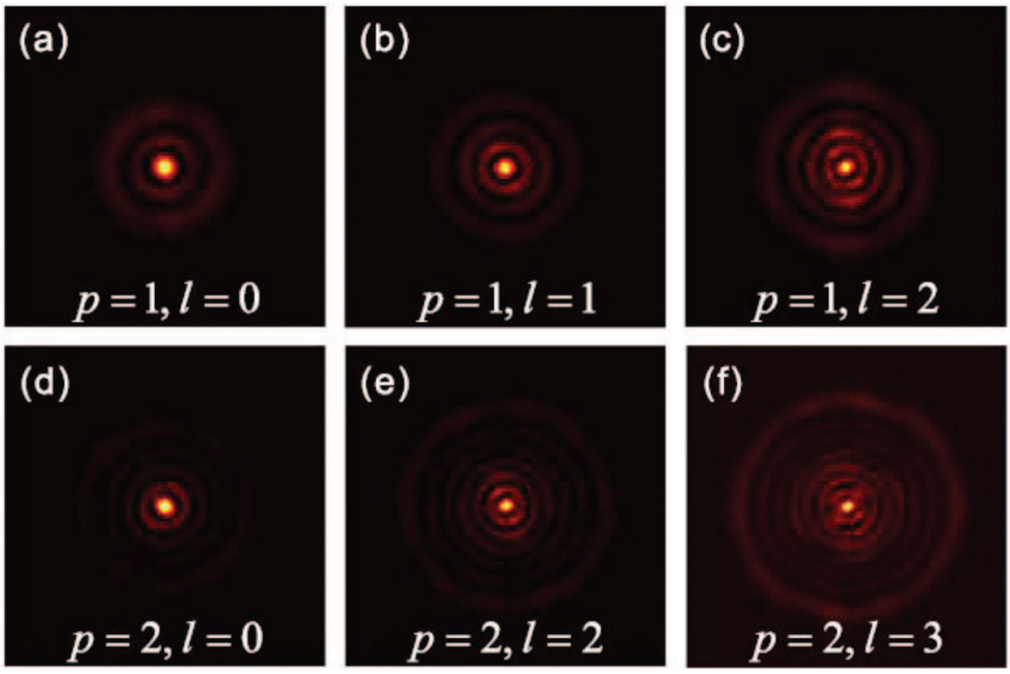

Figure 13. Experimental results of the distribution of the modulus of the degree of coherence of a partially coherent LG_{pl} beam in the focal plane for different values of p and l.

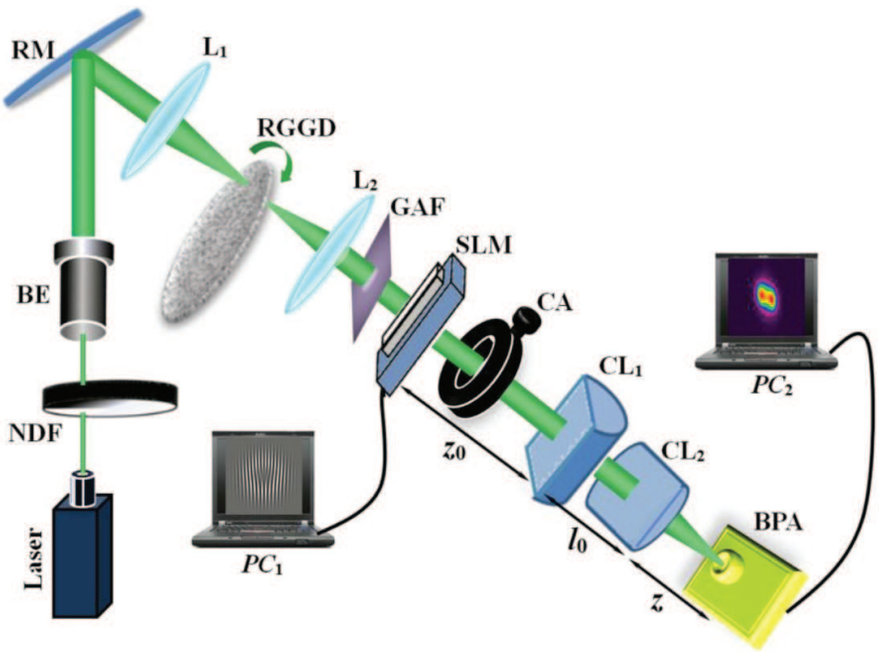

Figure 14. Experimental setup for determining the magnitude and the sign of the topological charge. NDF, neutral-density filter; BE, beam expander; RM, reflecting mirror; L_1, L_2, thin lenses; RGGD, rotating ground-glass disk; GAF, Gaussian amplitude filter; SLM, spatial light modulator; CA, circular aperture; CL_1, CL_2, cylindrical lenses; BPA, beam profile analyzer.

$2|l|+1$ (see **Figure 15**). One can extend this method to determine the sign and the magnitude of the topological charge of a partially coherent LG_{pl} beam based on the measurement of the double-correlation function.

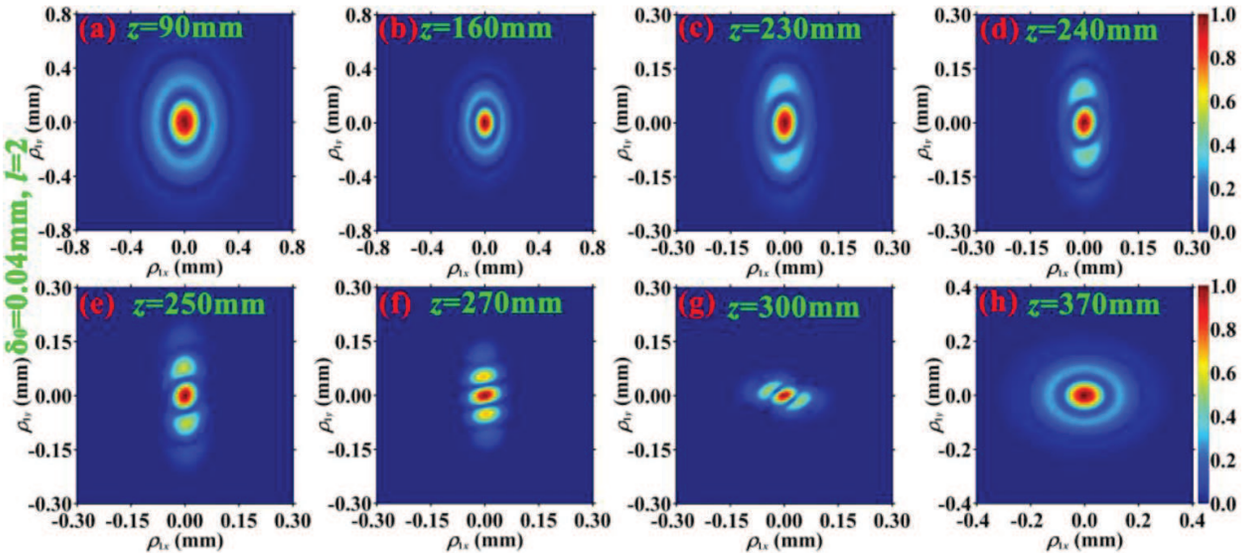

Figure 15. Distribution of the modulus of the degree of coherence of a partially coherent LG_{0l} beam after passing through a couple of cylindrical lenses at different propagation distances with l=2 and $\delta_0 = 0.04$mm.

6. Application of partially coherent vortex beams

Due to their extraordinary propagation properties, partially coherent vortex beams are useful in many applications, such as material processing, optical trapping, free-space optical communications and optical imaging.

It was shown in [46] that one can shape the beam profile of a focused partially coherent vortex beam through varying its initial spatial coherence width, and one can obtain flat-topped beam profile, dark hollow beam profile and Gaussian beam profile in the focal plane. The formed flat-topped beam profile is useful in material processing [91], and in trapping a Rayleigh particle whose refractive index is larger than that of the ambient [92], and the formed dark hollow beam profile is useful in trapping a Rayleigh particle whose refractive index is smaller than that of the ambient [72].

It is known that atmosphere turbulence induces scintillation of laser beam, which impedes the application of free-space optical communications. It was shown in [93] that partially coherent beam can be used to reduce turbulence-induced scintillation, and is useful in free-space optical communications [7, 8]. In [62], it was demonstrated experimentally a partially coherent vortex beam has an advantage over a partially coherent beam without vortex phase for reducing turbulence-induced scintillation, thus is expect to be useful in free-space optical communication.

Finally, we know that both partially coherent beam and vortex beam are useful in super-resolution imaging [94, 95], one may expect that partially coherent vortex beam has an advantage over partially coherent beam and vortex beam in super-resolution imaging. What is more, partially coherent vortex beam carries correlation singularities, and one may apply correlation singularities for information encoding, transfer and decoding.

7. Summary

We have presented on a review on recent theoretical and experimental developments on partially coherent vortex beam. The theoretical models, propagation properties, and generation methods for various partially coherent vortex beams have been illustrated in detail. Partially coherent vortex beams display many unique and interesting properties, and are useful in some applications, such as material processing, optical trapping, free-space optical communications and optical imaging. We believe this field will grow further and expand rapidly, and more and more interesting results and potential applications will be revealed.

Acknowledgements

This work is supported by the National Natural Science Fund for Distinguished Young Scholar under Grant no. 11525418, the National Natural Science Foundation of China under Grant no. 11404234 and 11274005, and the Project of the Priority Academic Program Development (PAPD) of Jiangsu Higher Education Institutions.

Author details

Xianlong Liu, Lin Liu, Yahong Chen and Yangjian Cai*

*Address all correspondence to: yangjiancai@suda.edu.cn

College of Physics, Optoelectronics and Energy & Collaborative Innovation Center of Suzhou Nano Science and Technology, Soochow University, Suzhou, China

References

[1] L. Mandel and E. Wolf, editors. *Optical Coherence and Quantum Optics*. Cambridge: Cambridge University Press; 1995.

[2] D. Kermisch. Partially coherent image processing by laser scanning. J. Opt. Soc. Am. 1975;**65**(8):887–891.

[3] Y. Cai and S. Zhu. Ghost imaging with incoherent and partially coherent light radiation. Phys. Rev. E. 2005;**71**(5):056607.

[4] T. E. Gureyev, D. M. Paganin, A. W. Stevenson, S. C. Mayo, and S. W. Wilkins. Generalized eikonal of partially coherent beams and its use in quantitative imaging. Phys. Rev. Lett. 2004;**93**(6):068103.

[5] C. Zhao, Y. Cai, and O. Korotkova. Radiation force of scalar and electromagnetic twisted Gaussian Schell-model beams. Opt. Express. 2009;**17**(24):21472–21487.

[6] Y. Dong, F. Wang, C. Zhao, and Y. Cai. Effect of spatial coherence on propagation, tight focusing and radiation forces of an azimuthally polarized beam. Phys. Rev. A. 2012;**86** (1):013840.

[7] J. C. Ricklin and F. M. Davidson. Atmospheric turbulence effects on a partially coherent Gaussian beam: implications for free-space laser communication. J. Opt. Soc. Am. A. 2002;**19**(9):1794–1802.

[8] F. Wang, X. Liu, and Y. Cai. Propagation of partially coherent beam in turbulent atmosphere: a review (invited review). Prog. Electromagn. Res. 2015;**150**:123–143.

[9] Y. Cai, O. Korotkova, H. T. Eyyuboğlu, and Y. Baykal. Active laser radar systems with stochastic electromagnetic beams in turbulent atmosphere. Opt. Express. 2008;**16** (20):15834–15846.

[10] O. Korotkova, Y. Cai, and E. Watson. Stochastic electromagnetic beams for LIDAR systems operating through turbulent atmosphere. Appl. Phys. B. 2009;**94**(4):681–690.

[11] G. Wu and Y. Cai. Detection of a semirough target in turbulent atmosphere by a partially coherent beam. Opt. Lett. 2011;**36**(10):1939–1941.

[12] E. Wolf and E. Collett. Partially coherent sources which produce the same far-field intensity distribution as a laser. Opt. Commun. 1978;**25**(3):293–296.

[13] F. Gori. Collet–Wolf sources and multimode lasers. Opt. Commun. 1980;**34**(3):301–305.

[14] P. de Santis, F. Gori, G. Guattari, and C. Palma. An example of a Collett–Wolf source. Opt. Commun. 1979;**29**(3):256–260.

[15] A. T. Friberg and R. J. Sudol. Propagation parameters of Gaussian Schell-model beams. Opt. Commun. 1982;**41**(6):383–387.

[16] E. Tervonen, A. T. Friberg, and J. Turunen. Gaussian Schell-model beams generated with synthetic acousto-optic holograms. J. Opt. Soc. Am. A. 1992;**9**(5):796–803.

[17] E. Wolf, editor. *Introduction to the Theory of Coherence and Polarization of Light*. Cambridge: Cambridge University; 2007.

[18] Y. Cai. Generation of various partially coherent beams and their propagation properties in turbulent atmosphere: a review. Proc. of SPIE. 2011;**7924**:792402.

[19] Y. Cai, Y. Chen, and F. Wang. Generation and propagation of partially coherent beams with nonconventional correlation functions: a review [invited]. J. Opt. Soc. Am. A. 2014;**31**(9):2083–2096.

[20] Y. Cai, F. Wang, C. Zhao, S. Zhu, G. Wu, and Y. Dong. Partially coherent vector beams: from theory to experiment. In: Q. Zhan, editor. *Vectorial Optical Fields: Fundamentals and Applications*. 1st ed. Singapore: World Scientific; 2013. pp. 221–273.

[21] F. Gori, M. Santarsiero, G. Piquero, R. Borghi, A. Mondello, and R. Simon. Partially polarized Gaussian schell model beams. J. Opt. A, Pure Appl. Opt. 2001;**3**(1):1–9.

[22] E. Wolf. Unified theory of coherence and polarization of random electromagnetic beams. Phys. Lett. A. 2003;**312**(5):263–267.

[23] O. Korotkova and E. Wolf. Changes in the state of polarization of a random electromagnetic beam on propagation. Opt. Commun. 2005;**246**(1):35–43.

[24] H. Roychowdhury, S. A. Ponomarenko, and E. Wolf. Change in the polarization of partially coherent electromagnetic beams propagating through the turbulent atmosphere. J. Mod. Opt. 2005;**52**(11):1611–1618.

[25] H. Lajunen and T. Saastamoinen. Non-uniformly correlated partially coherent pulses. Opt. Lett. 2013;**21**(1):190–195.

[26] S. Sahin and O. Korotkova. Light sources generating far fields with tunable flat profiles. Opt. Lett. 2012;**37**(4):2970–2972.

[27] F. Wang, X. Liu, Y. Yuan, and Y. Cai. Experimental generation of partially coherent beams with different complex degrees of coherence. Opt. Lett. 2013;**38**(11):1814–1816.

[28] C. Liang, F. Wang, X. Liu, Y. Cai, and O. Korotkova. Experimental generation of cosine Gaussian-correlated Schell-model beams with rectangular symmetry. Opt. Lett. 2014;**39**(4):769–772.

[29] O. Korotkova. Random sources for rectangularly-shaped far fields. Opt. Lett. 2014;**39**(1):64–67.

[30] Y. Chen, F. Wang, L. Liu, C. Zhao, Y. Cai, and O. Korotkova. Generation and propagation of a partially coherent vector beam with special correlation functions. Phys. Rev. A. 2014;**89**(1):013801.

[31] Y. Chen, J. Gu, F. Wang, and Y. Cai. Self-splitting properties of a Hermite-Gaussian correlated Schell-model beam. Phys. Rev. A. 2015;**91**(1):013823.

[32] L. Allen, M. W. Beijersbergen, R. Spreeuw, and J. P. Woerdman. Orbital angular momentum of light and the transformation of Laguerre-Gaussian laser modes. Phys. Rev. A. 1992;**4**(11):8185–8189.

[33] L. Allen, M. J. Padgett, and M. Babiker. The orbital angular momentum of light. Prog. Opt. 1999;39:291–372.

[34] H. He, M. E. J. Friese, N. R. Heckenberg, and H. Rubinsztein-Dunlop. Direct observation of transfer of angular momentum to absorptive particles from a laser beam with a phase singularity. Phys. Rev. Lett. 1995;**75**(5):826–829.

[35] T. Kuga, Y. Torii, N. Shiokawa, T. Hirano, Y. Shimizu, and H. Sasada. Novel optical trap of atoms with a doughnut beam. Phys. Rev. Lett. 1997;**78**(25):4713–4716.

[36] D. G. Grier. A revolution in optical manipulation. Nature. 2003;**424**(6950):810–816.

[37] G. Molina-Terriza, J. P. Torres, and L. Torner. Twisted photons. Nat. Phys. 2007;**3**(5):305–310.

[38] A. Mair, A. Vaziri, G. Weighs, and A. Zeilinger. Entanglement of the orbital angular momentum states of photons. Nature. 2001;**412**(6844):313–316.

[39] J. Ng, Z. Lin, and C. T. Chan. Theory of optical trapping by an optical vortex beam. Phys. Rev. Lett. 2010;**104**(10):103601.

[40] J. Wang, J. Yang, I. M. Fazal, N. Ahmed, Y. Yan, H. Huang, Y. Ren, Y. Yue, S. Dolinar, M. Tur, and A. E. Willner. Terabit free-space data transmission employing orbital angular momentum multiplexing. Nat. Photonics. 2012;**6**(7):488–496.

[41] E. Nagali, F. Sciarrino, F. De Martini, L. Marrucci, B. Piccirillo, E. Karimi, and E. Santamato. Quantum information transfer from spin to orbital angular momentum of photons. Phys. Rev. Lett. 2009;**103**(1):013601.

[42] M. P. J. Lavery, F. C. Speirits, S. M. Barnett, and M. J. Padgett. Detection of a spinning object using light's orbital angular momentum. Science. 2013;**341**(6145):537–540.

[43] F. Gori, M. Santarsiero, R. Borghi, and S. Vicalvi. Partially coherent sources with helicoidal modes. J. Mod. Opt. 1998;**45**(3):539–554.

[44] V. G. Boggatyryova, V. C. Felde, P. V. Polyanskii, S. A. Ponomarenko, M. S. Soskin, and E. Wolf. Partially coherent vortex beams with a separable phase. Opt. Lett. 2003;**28**(11):878–880.

[45] S. A. Ponomarenko. A class of partially coherent beams carrying optical vortices. J. Opt. Soc. Am. A. 2001;**18**(1):150–156.

[46] F. Wang, S. Zhu, and Y. Cai. Experimental study of the focusing properties of a Gaussian Schell-model vortex beam. Opt. Lett. 2011;**36**(16):3281–3283.

[47] D. Palacios, I. Maleev, A. Marathay, and G. A. Swartzlander. Spatial correlation singularity of a vortex field. Phys. Rev. Lett. 2004;**92**(14):143905.

[48] C. Zhao, Y. Dong, Y. Wang, F. Wang, Y. Zhang, Y. Cai. Experimental generation of a partially coherent Laguerre-Gaussian beam. Appl. Phys. B. 2012;**109**(2):345–349.

[49] F. Wang, Y. Cai, and O. Korotkova. Partially coherent standard and elegant Laguerre-Gaussian beams of all orders. Opt. Express. 2009;**17**(25):22366–22379.

[50] Z. Zhang, J. Pu, and X. Wang. Focusing of partially coherent Bessel-Gaussian beams through a high-numerical-aperture objective. Opt. Lett. 2008;**33**(1):49–51.

[51] Y. Chen, F. Wang, C. Zhao, and Y. Cai. Experimental demonstration of a Laguerre-Gaussian correlated Schell-model vortex beam. Opt. Express. 2014;22(5):5826–5838.

[52] Y. Zhang, L. Liu, C. Zhao, and Y. Cai. Multi-Gaussian Schell-model vortex beam. Phys. Lett. A. 2014;**378**(9):750–754.

[53] X. Liu, F. Wang, L. Liu, C. Zhao, and Y. Cai. Generation and propagation of an electromagnetic Gaussian Schell-model vortex beam. J. Opt. Soc. Am. A. 2015;**32**(11):2058–2065.

[54] L. Guo, Y. Chen, X. Liu, L. Liu, and Y. Cai. Vortex phase-induced changes of the statistical properties of a partially coherent radially polarized beam. Opt. Express. 2016;**24** (13):13714–13728.

[55] I. D. Maleev, D. M. Palacios, A. S. Marathay, and G. A. Swartzlander. Spatial correlation vortices in partially coherent light: theory. J. Opt. Soc. Am. B. 2004;**21**(11):1895–1900.

[56] T. Van Dijk and T. D. Visser. Evolution of singularities in a partially coherent vortex beam. J. Opt. Soc. Am. A. 2009;**26**(4):741–744.

[57] I. D. Maleev and G. A. Swartzlander. Propagation of spatial correlation vortices. J. Opt. Soc. Am. B. 2008;**25**(6):915–922.

[58] W. Wang, M. Takeda. Coherence current, coherence vortex, and the conservation law of coherence. Phys. Rev. Lett. 2006;**96**(22):223904.

[59] W. Wang, Z. Duan, S. G. Hanson, Y. Miyamoto, and M. Takeda. Experimental study of coherence vortices: Local properties of phase singularities in a spatial coherence function. Phys. Rev. Lett. 2006;**96**(7):073902.

[60] Y. Zhang, M. Tang, and C. Tao. Partially coherent vortex beams propagating in a turbulent atmosphere. Chin. Opt. Lett. 2005;**3**(10):559–561.

[61] F. Wang, Y. Cai, H. Eyyuboglu, and Y. Baykal. Average intensity and spreading of partially coherent standard and elegant Laguerre-Gaussian beams in turbulent atmosphere. Prog. Electromagn. Res. 2010;**103**:33–56.

[62] X. Liu, Y. Shen, L. Liu, F. Wang, and Y. Cai. Experimental demonstration of vortex phase-induced reduction in scintillation of a partially coherent beam. Opt. Lett. 2013;**38** (24):5323–5326.

[63] H. Pires, J. Woudenberg, and M. Van Exter. Measurements of spatial coherence of partially coherent light with and without orbital angular momentum. J. Opt. Soc. Am. A. 2010;**27**(12):2630–2637.

[64] H. Pires, J. Woudenberg, and M. Van Exter. Measurement of the orbital angular momentum spectrum of partially coherent beams. Opt. Lett. 2010;**35**(6):889–891.

[65] C. Zhao, F. Wang, Y. Dong, Y. Han and Y. Cai. Effect of spatial coherence on determining the topological charge of a vortex beam. Appl. Phys. Lett. 2012;**101**(26):261104.

[66] Y. Yang, M. Mazilu, and K. Dholakia. Measuring the orbital angular momentum of partially coherent optical vortices through singularities in their cross-spectral density functions. Opt. Lett. 2012;**37**(23):4949–4951.

[67] A. Y. Escalante, B. Perez-Garcia, R. I. Hernandez-Aranda, and G. A. Swartzlander. Determination of angular momentum content in partially coherent beams through cross correlation measurements. Proc. SPIE. 2013;**8843**:884302.

[68] Y. Yang, M. Chen, M. Mazilu, A. Mourka, Y. Liu and K. Dholakia. Effect of the radial and azimuthal mode indices of a partially coherent vortex field upon a spatial correlation singularity. New J. Phys. 2013;**15**(11):113053.

[69] R. Liu, F. Wang, D. Chen, Y. Wang, Y. Zhou, H. Gao, P. Zhang, and F. Li. Measuring mode indices of a partially coherent vortex beam with Hanbury Brown and Twiss type experiment. App. Phys. Lett. 2016;**108**(5):051107.

[70] Y. Yang and Y. Liu. Measuring azimuthal and radial mode indices of a partially coherent vortex field. J. Opt. 2016;**18**(1):015604.

[71] J. Chen, X. Liu, J. Yu, and Y. Cai. Simultaneous determination of the sign and the magnitude of the topological charge of a partially coherent vortex beam. App. Phys. B. 2016;**122**:201

[72] C. Zhao and Y. Cai. Trapping two types of particles using a focused partially coherent elegant Laguerre-Gaussian beam. Opt. Lett. 2011;**36**(12):2251–2253.

[73] B. Perez-Garcia, A. Yepiz, R. I. Hernandez-Aranda, A. Forbes, and G. A. Swartzlander. Digital generation of partially coherent vortex beams. Opt. Lett. 2016; **41**(15):3471–3474.

[74] Q. Lin and Y. Cai. Tensor ABCD law for partially coherent twisted anisotropic Gaussian-Schell model beams. Opt. Lett. 2002;**27**(4):216–218.

[75] S. C. H. Wang and M. A. Plonus. Optical beam propagation for a partially coherent source in the turbulent atmosphere. J. Opt. Soc. Am. 1979;**69**(9):1297–1304.

[76] K. Sueda, G. Miyaji, N. Miyanaga, M. Nakatsuka. Laguerre-Gaussian beam generated with a multilevel spiral phase plate for high intensity laser pulses. Opt. Express. 2004;**12** (15):3548–3553.

[77] M. Vaupel and C. O. Weiss. Circling optical vortices. Phys. Rev. A. 1995;**51**(5):4078–4085.

[78] N. R. Heckenberg, R. McDuff, C. P. Smith, and A. G. White. Generation of optical phase singularities by computer-generated holograms. Opt. Lett. 1992;**17**(3):221–223.

[79] J. B. Bentley, J. A. Davisa, M. A. Bandres, and J. C. Guti_errez-Vega. Generation of helical Ince Gaussian beams with a liquid-crystal display. Opt. Lett. 2006;**31**(5):649–651.

[80] C. N. Alexeyev and M. A. Yavorsky. Generation and conversion of optical vortices in long-period helical core optical fibers. Phys. Rev. A. 2008;**78**(4):043828.

[81] A. Volyar, V. Shvedov, T. Fadeyeva, A. S. Desyatnikov, D. N. Neshev, W. Krolikowski, and Yu. S. Kivshar. Generation of single-charge optical vortices with an uniaxial crystal. Opt. Express. 2006;**14**(9):3724–3729.

[82] V. Denisenko, V. Shvedov, A. S. Desyatnikov, D. N. Neshev, W. Krolikowski, A. Volyar, M. Soskin, and Y. S. Kivsar. Determination of topological charges of polychromatic optical vortices. Opt. Express. 2009;**17**(26):23374–23379.

[83] G. C. G. Berkhout and M. W. Beijersbergen. Method for probing the arbital angular momentum of optical vortices in electromagnetic waves from astronomical objects. Phys. Rev. Lett. 2008;**101**(10):100801.

[84] J. M. Hickmann, E. J. S. Fonseca, W. C. Soares, and S. Chávez-Cerda. Unveiling a truncated optical lattice associated with a triangular aperture using light's orbital angular momentum. Phys. Rev. Lett. 2010;**105**(5):053904.

[85] R. Liu, J. Long, F. Wang, Y. Wang, P. Zhang, H. Gao and F. Li. Characterizing the phase profile of a vortex beam with angular-double-slit interference. J. Opt. 2013;**15**(12):125712.

[86] D. Fu, D. Chen, R. Liu, Y. Wang, H. Gao, F. Li, and P. Zhang. Probing the topological charge of a vortex beam with dynamic angular double slits. Opt. Lett. 2015;**40**(5):788–791.

[87] G. C. G. Berkhout, M. P. J. Lavery, J. Courtial, M. W. Beijersbergen, and M. J. Padgett. Efficient sorting of orbital angular momentum states of light. Phys. Rev. Lett. 2010;**105** (15):153601.

[88] S. Prabhakar, A. Kumar, J. Banerji, and R. P. Singh. Revealing the order of a vortex through its intensity record. Opt. Lett. 2011;**36**(22):4398–4400.

[89] N. Bozinovic, Y. Yue, Y. X. Ren, M. Tur, P. Kristensen, H. Huang, A. E. Willner, and S. Ramachandran. Terabit-scale orbital angular momentum mode division multiplexing in fibers. Science. 2013;**340**(6140):1545–1548.

[90] Y. Ming, J. Tang, Z. Chen, F. Xu, L. Zhang, and Y. Lu. Generation of n00n state with orbital angular momentum in a twisted nonlinear photonic crystal. IEEE. J. Quantum Electron. 2015;**21**(3):6601206.

[91] D. W. Coutts. Double-pass copper vapor laser master-oscillator power-amplifier systems: Generation of flat-top focused beams for fiber coupling and percussion drilling. IEEE J. Quantum Electron. 2002;**38**(9):1217–1224.

[92] C. Zhao, Y. Cai, X. Lu, and H. T. Eyyuboğlu. Radiation force of coherent and partially coherent flat-topped beams on a Rayleigh particle. Opt. Express. 2009;**17**(3):1753–1765.

[93] Y. Baykal and M. A. Plonus. Intensity fluctuations due to a spatially partially coherent source in atmospheric turbulence as predicted by Rytov's method. J. Opt. Soc. Am. A. 1985;**2**(12):2124–2132.

[94] F. Tamburini, G. Anzolin, G. Umbriaco, A. Bianchini, and C. Barbieri. Overcoming the Rayleigh criterion limit with optical vortices. Phys. Rev. Lett. 2006;**97**(16):163903.

[95] J. E. Oh, Y. W. Cho, G. Scarcelli, and Y. H. Kim. Sub-Rayleigh imaging via speckle illumination. Opt. Lett. 2013;**38**(5):682–684.